Finite element simulation of Rayleigh surface acoustic wave in (100) AlN/(100) ZnO/diamond layered structure*

ZHANG Zeyu[1,2], QIAN Jin[1,2], QIAN Lirong[1,2], WEN Fujun[1,2], WANG Litian[1,2], and LI Cuiping[1,2]****

1. *Tianjin Key Laboratory of Film Electronic and Communication Devices, School of Integrated Circuit Science and Engineering, Tianjin University of Technology, Tianjin 300384, China*
2. *Engineering Research Center of Optoelectronic Devices & Communication Technology, School of Integrated Circuit Science and Engineering, Tianjin University of Technology, Tianjin 300384, China*

(Received 14 April 2023; Revised 31 May 2023)

With the rapid development of the fifth-generation (5G) wireless system, the explosive growth of transmitted data raises higher requirements for high-performance surface acoustic wave (SAW) devices as filters and duplexers. (100) AlN/(100) ZnO/diamond layered structures are theoretically simulated by finite element method (FEM) to investigate the Rayleigh SAW propagation properties, including phase velocity, electromechanical coupling coefficient K^2, and temperature coefficient of frequency (*TCF*). Three types of layered structures with different interdigital transducers (IDTs) arrangements, which are IDTs/(100) AlN/(100) ZnO/diamond, (100) AlN/IDTs/(100) ZnO/diamond, and (100) AlN/(100) ZnO/IDTs/diamond structures, are considered in the simulations. The results show that the Sezawa mode exhibits larger K^2 than the other modes. We found that the (100) AlN/IDTs/(100) ZnO/diamond structure exhibited better SAW properties, including high K^2 and appropriate phase velocity.

Document code: A **Article ID:** 1673-1905(2023)12-0732-7
DOI https://doi.org/10.1007/s11801-023-3071-4

Surface acoustic wave (SAW) devices have been widely used in the field of wireless communication due to their small size, low cost, and stable performance. They are the key components of mobile communication systems and dominate the fourth-generation (4G) wireless application market. With the rapid popularization of the fifth-generation (5G) mobile communication systems, mobile data has grown explosively, which puts forward higher requirements for the performance of SAW devices, such as higher frequencies, wider bandwidth, smaller losses, smaller dimensions, and better temperature stability[1-4]. The performances of SAW devices are determined by the sound velocity, electromechanical coupling coefficient, and frequency temperature coefficient of the substrate material. Traditional SAW devices based on piezoelectric single crystals are no longer able to meet these requirements. SAW devices with multi-layered structures containing ultra-high sound velocity substrates (such as diamond and SiC) have received increasing attention[5-7]. For example, LI et al[8] reported a high performance SAW resonator based on $LiTaO_3/SiO_2/SiC$ multilayer structure. SHEN et al[2] simulated and fabricated a high performance SAW filter based on $LiNbO_3/SiO_2/SiC$ multilayer structure. Among all materials, diamond has the highest sound velocity, but diamond is not a piezoelectric material and needs to be combined with piezoelectric materials. ZnO and AlN films are the common used piezoelectric films in layered structures[9]. ZnO possesses relatively large piezoelectric coefficients and therefore can exhibit a high electromechanical coupling coefficient (K^2). However, the acoustic phase velocity of ZnO is low[10]. On the other hand, AlN exhibits a low K^2 but a relatively high velocity. Given the advantages of ZnO and AlN, ZnO/AlN/diamond, AlN/ZnO/diamond and $(AlN/ZnO)_N$/diamond structures were proposed to balance the velocity and K^2[11,12].

The excitation and propagation properties of SAW for layered structures are greatly influenced by the crystal orientations of piezoelectric films[13]. Rayleigh SAW with a mechanical displacement component perpendicular to the substrate surface is the first studied and widely used SAW. Both (002) and (100) oriented ZnO (or AlN) films can excite the Rayleigh SAW on different substrates[14,15]. It is reported that Rayleigh SAW in (100) ZnO/diamond structure possesses the larger coupling coefficients than those in the (002) ZnO/diamond one and the similar regularity was also found to (100) AlN/diamond and (002) AlN/diamond structures. The

* This work has been supported by the Research and Development Program in Significant Area of Guangdong Province (No.2020B0101040002), the Guangzhou Key Research & Development Program, Major Science and Technology Projects (No.202206070001), the National Natural Science Foundation of China (No.62271350), and the Natural Science Foundation of Tianjin (No.20JCZDJC00290).
** E-mails: qianlirong83@163.com; licp226@126.com

maxima K^2 value of Rayleigh SAW for interdigital transducers (IDT)/(002) ZnO/diamond structure is 2.69% while for IDT/(100) ZnO/diamond structure is 4.28%[15]. The optimal K^2 value for IDT/(002) AlN/diamond structure is 1.24% while for IDT/(100) ZnO/diamond structure is 2.31%[14]. The Rayleigh SAW in (100) ZnO/IDT/(100) AlN/diamond structure was also investigated and found that a high K^2 of 6.05% associated with a phase velocity of 6 234 m/s can be obtained[13]. The SAW properties are closely related to the arrangement order of the piezoelectric films and IDTs in layered structure[16]. To the best of our knowledge, the SAW properties in (100) AlN/(100) ZnO/diamond structure has not been study systematically. With the development of film preparation technology, (100) AlN and (100) ZnO films have been successfully, confirming the feasibility of this structure[17-25].

In this work, the SAW propagation properties are simulated by finite element method (FEM) based on (100) AlN/(100) ZnO/diamond layered structures[26]. Three types of IDTs arrangements, as shown in Fig.1, are considered in the calculation. The effects of the thickness ratios of AlN film to ZnO film (R_h) in the three structures are also discussed.

Fig.1 is the illustration of (100) AlN/(100) ZnO/diamond structures with three types of IDTs arrangements under global Cartesian coordinate system (x, y, z). The direction of z axis is perpendicular to the substrate surface and also is the normal direction of (100) crystal planes of the ZnO and AlN. The SAW propagates along the x direction, which is also the (001) crystal planes of the ZnO and AlN. The finger width is 1.0 μm, and the wavelength λ is 4 μm. The thickness of the IDTs is 40 nm. The thickness of the ZnO film is denoted by h_{ZnO} and that of AlN film by h_{AlN}. R_h represents the ratio of h_{AlN} to h_{ZnO} and H is the total thickness of ZnO and AlN films. The coupled wave equations satisfied by SAW are shown as

$$\begin{cases} c_{ijkl}^{E}\dfrac{\partial^2 u_k}{\partial x_l \partial x_j}+e_{kij}\dfrac{\partial^2 \Phi}{\partial x_k \partial x_j}=\rho\dfrac{\partial^2 u_i}{\partial t^2} \\ e_{ikl}\dfrac{\partial^2 u_k}{\partial x_l \partial x_i}-\varepsilon_{ik}^{S}\dfrac{\partial^2 \Phi}{\partial x_k \partial x_i}=0 \end{cases}, \tag{1}$$

where u_i is the displacement, Φ is the electrical potential (V), c_{ijkl}^{E} is the elastic tensor (N/m^2), e_{kij} is the piezoelectric tensor (C/m^2), ε_{ik}^{S} is the dielectric tensor (F/m), and ρ is the mass density (kg/m^3). A commercial FEM software of COMSOL Mutiphysics was used to simulated the SAW characteristics in the layered structure. The material parameters of diamond, (100) ZnO, (100) AlN, and Al are listed in Tab.1.

The input admittance is calculated by applying a sinusoidal voltage signal to the IDTs. The resonance frequency (f_{r}) and the anti-resonance frequency (f_{ar}) are determined from the input admittance. The phase velocity of SAW is calculated using the following equation[26]

$$v=\lambda f_{\mathrm{r}}. \tag{2}$$

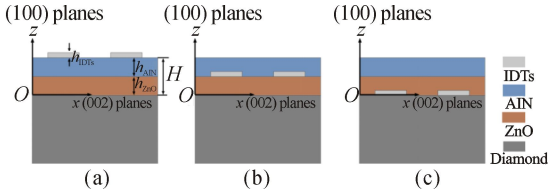

Fig.1 Illustration of (100) AlN/(100) ZnO/diamond structures with three types of IDTs arrangements considered in the calculation: (a) IDTs/(100) AlN/(100) ZnO/diamond; (b) (100) AlN/IDTs/(100) ZnO/diamond; (c) (100) AlN/(100) ZnO/IDTs/diamond (Coordinate system and crystal axes are also given)

Tab.1 Material constants and temperature coefficients used in the calculation

	Symbol	Diamond	(100) ZnO	(100) AlN	Al
Elastic constants (10^{11} N/m^2)	c_{11}	11.531	2.106	3.95	1.11
	c_{12}	0.864	1.046	1.2	0.59
	c_{13}	0.864	1.046	1.2	0.59
	c_{33}	11.531	2.096	3.45	1.11
	c_{44}	5.333	0.445 5	1.1	0.26
Temperature coefficients of elastic constants (10^{-4}/°C)	T_{c11}	−0.14	−1.23	−0.65	−5.9
	T_{c13}	−0.57	−1.61	−0.018	−0.8
	T_{c33}	−0.14	−1.21	−0.37	−5.9
	T_{c44}	−0.125	−0.48	−0.57	−5.2
Piezoelectric constants (C/m^2)	e_{11}	---	1.321	1.55	---
	e_{12}	---	−0.573	−0.58	---
	e_{13}	---	−0.573	−0.58	---
	e_{26}	---	−0.48	−0.48	---
	e_{35}	---	−0.48	−0.48	---
Relative dielectric constants	$\varepsilon_{11}/\varepsilon_0$	5.67	10.2	10.73	1
	$\varepsilon_{33}/\varepsilon_0$	5.67	8.55	9.04	1
Mass density (10^3 kg/m^3)	ρ	3.512	5.665	3.26	2.7
Temperature coefficients of mass density (10^{-6}/°C)	T_ρ	−3.6	−10.1	−14.69	−1.65

The electromechanical coupling coefficient K^2 is an important performance index that can evaluate the conversion efficiency of acoustic-electric transformation, which can be estimated from the following equation[27]

$$K^2 \approx 2\frac{f_{\mathrm{ar}}-f_{\mathrm{r}}}{f}. \tag{3}$$

The temperature coefficient of frequency (*TCF*) is another important performance parameter to evaluate the temperature stability of the SAW devices. A *TCF* close to 0 is expected for many SAW device applications, such as wireless communications and sensor. *TCF* is obtained as follows[28]

$$TCF = \frac{1}{f_r}\frac{\partial f_r}{\partial T}, \tag{4}$$

where T is the temperature.

Fig.2 shows the admittance curves for the three types of layered structures considered in the calculation as a function of driving frequency. The normalized thickness of H (H/λ) is fixed at 0.5 and the R_h is 1, which are the same for the three structures. Excite modes of SAW can be easily identified from the peaks in the admittance curves. The three peaks correspond to the first three modes, the fundamental mode (M0) and its higher modes (M1 and M2), of which the M0 with the lowest resonance frequency is called Rayleigh mode, while the M1 is called Sezawa mode.

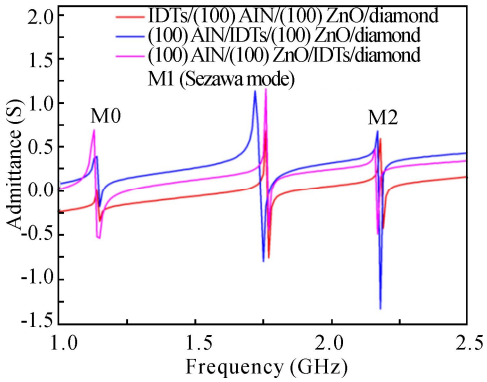

Fig.2 Input admittances of three types of layered structures considered in the calculation with R_h=1 and H/λ=0.5

The dispersion behaviors of phase velocity and K^2 were calculated for the three structures with different IDTs arrangements. Fig.3 shows the dispersion curves for the first three modes as a function of H/λ. The R_h is fixed to 1 for the three structures. The Sezawa mode can be observed when the H/λ exceeds 0.13 and the M2 is found at the H/λ higher than 0.2. In Figs.3(a—c), a higher phase velocity can be obtained for the higher order mode at the same H/λ. The positions of the IDTs have little influence on the phase velocity for all the three modes. However, the K^2 values are greatly influenced by the positions of the IDTs, as shown in Figs.3(d—f). For the IDTs/(100) AlN/(100) ZnO/diamond structure, the K^2 values of M0 and M2 are both relatively low while those of the Sezawa mode (M1) are relatively large when the range of H/λ value is from 0.15 to 0.40. In the case of the (100) AlN/IDTs/(100) ZnO/diamond structure, the Sezawa mode has a much larger value of K^2 than the other modes in our research range of H/λ. As for the (100) AlN/(100) ZnO/IDTs/diamond structure, the Sezawa mode has a relatively large value of K^2 at H/λ lower than 0.25 and the M1 has a relatively large K^2 at H/λ larger than 0.25.

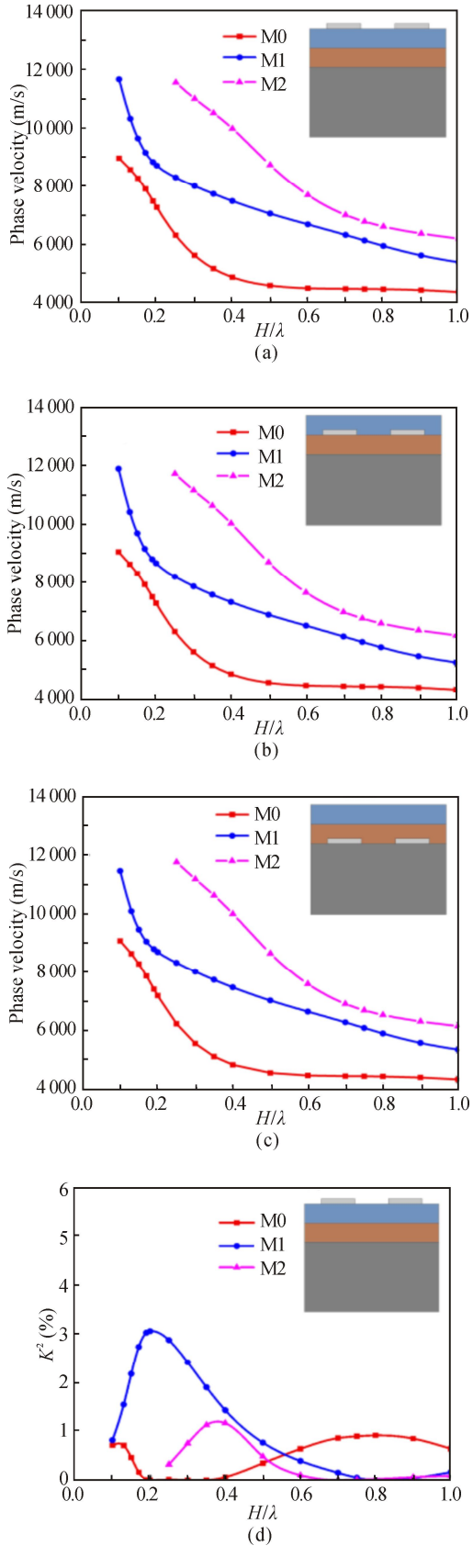

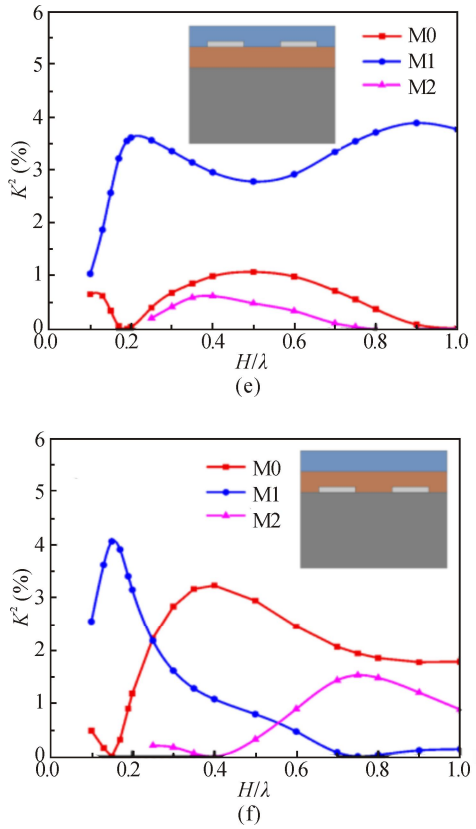

Fig.3 (a—c) Phase velocity and (d—f) K^2 curves of the first three Rayleigh modes as a function of the normalized piezoelectric films total thickness H/λ for the three structures with different IDTs positions: (a, d) IDTs/(100) AlN/(100) ZnO/diamond; (b, e) (100) AlN/IDTs/(100) ZnO/diamond; (c, f) (100) AlN/(100) ZnO/IDTs/diamond (The ratio R_h of h_{AlN} to h_{ZnO} is 1 for the three structures)

Consider that Sezawa mode of SAW shows relatively large K^2 in the three considered structures. The velocity, K^2, and *TCF* of the Sezawa mode are investigated in detail as a function of H/λ at different R_h. Fig.4 displays the phase velocity, K^2, and *TCF* curves for the Sezawa SAW in the IDTs/(100) AlN/(100) ZnO/diamond structure. IDTs/(100) ZnO/diamond and IDTs/(100) AlN/diamond structures are two extreme cases for the IDTs/(100) AlN/(100) ZnO/dia-mond structure when the R_h ratio equal to 0 and infinity, respectively. For comparison, the phase velocity, K^2, and *TCF* curves of the IDTs/(100) ZnO/diamond structure and the IDTs/(100) AlN/diamond structure are also presented in Fig.4. From Fig.4(a), the phase velocity of IDTs/(100) AlN/(100) ZnO/diamond structure is between those of IDTs/(100) ZnO/diamond and IDTs/(100) AlN/diamond structures, and the phase velocity decreases with increasing H/λ but increases as the R_h increases. Moreover, the phase velocity curves exhibit a higher dispersion when the H/λ is smaller than 0.2 but a lower dispersion when the H/λ is larger than 0.2. The similar variations were also observed in (002) AlN/(002) ZnO/diamond structure[8]. The K^2 values of the Sezawa mode in the IDTs/(100) AlN/(100) ZnO/diamond structure depend not only on the H/λ but also on the R_h, as shown in Fig.4(b). The K^2 values first increase to the maximum and then decrease as H/λ increasing for different R_h rations. The larger K^2 can be obtained for lower R_h due to the better piezoelectricity of ZnO than that of AlN. It is worth mentioning that for the H/λ value less than 0.2, the K^2 for the IDTs/(100) AlN/(100) ZnO/diamond structure are larger than those of IDTs/(100) ZnO/diamond structure. The *TCF* of the Sezawa mode is improved with R_h increasing, as shown in Fig.4(c), because AlN, comparing with ZnO, has the lower *TCF* absolute value. Noticing that the *TCF* absolute value in IDTs/(100) AlN/(100) ZnO/diamond structure can be lower than those in the IDTs/(100) AlN/diamond sturcture.

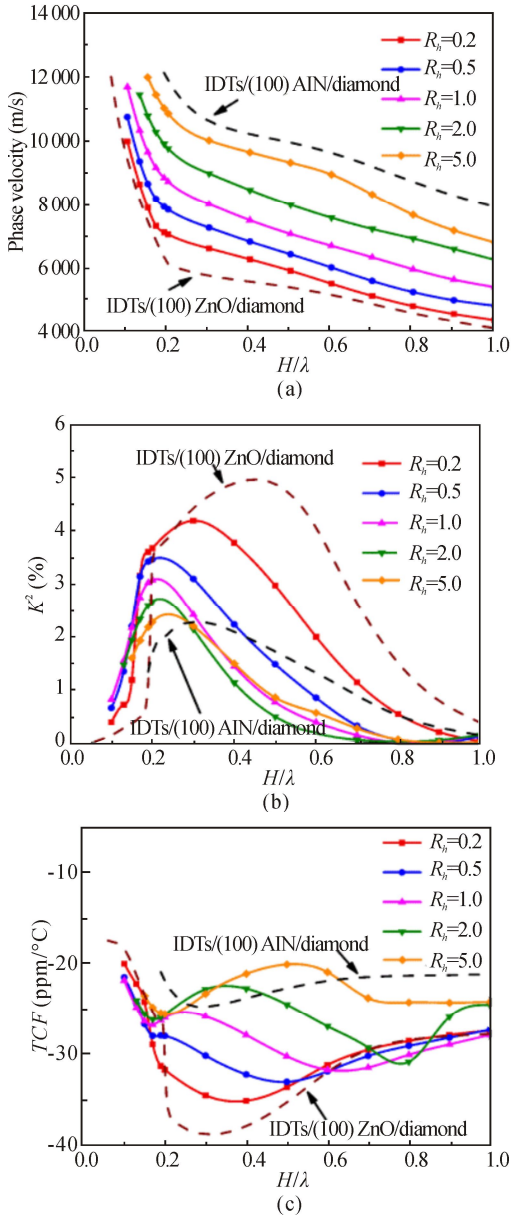

Fig.4 Calculated (a) phase velocity, (b) K^2, and (c) *TCF* for the Sezawa mode of SAW as a function of the H/λ in the IDTs/(100) AlN/(100) ZnO/diamond structure with different ratios of h_{AlN} to h_{ZnO}

The phase velocity, K^2, and *TCF* curves of the Sezawa mode SAW in the (100) AlN/IDTs/(100) ZnO/diamond structure is shown in Fig.5 as a function of H/λ at different R_h. Two extreme cases for the (100) AlN/IDTs/(100) ZnO/diamond structure when the R_h ratio equal to 0 and infinity respectively are IDTs/(100) ZnO/diamond and (100) AlN/IDTs/diamond structures. The corresponding data of IDTs/(100) ZnO/diamond and (100) AlN/IDTs/diamond structures are also added in Fig.5 for comparison. The phase velocity curves of (100) AlN/IDTs/(100) ZnO/diamond structure, as shown in Fig.5(a), are similar to those of IDTs/(100) AlN/(100) ZnO/diamond structure in Fig.4(a). The *TCF* curves of (100) AlN/IDTs/(100) ZnO/diamond structure in Fig.5(c) are slightly improved, comparing with those of IDTs/(100) AlN/(100) ZnO/diamond structure in Fig.4(c). For instance, the *TCF* is −20.1 ppm/°C for IDTs/(100) AlN/(100) ZnO/diamond structure and 18.5 ppm/°C for (100) AlN/IDTs/(100) ZnO/diamond structure when the H/λ is 0.45 and R_h is 5.0. The K^2 values of (100) AlN/IDTs/(100) ZnO/diamond structure show high values at wide range of H/λ, as shown in Fig.5(b), which are higher than those of IDTs/(100) AlN/(100) ZnO/diamond and IDTs/(100) ZnO/diamond structures. The maximum K^2 of 5.2% is obtained at H/λ=0.35 and R_h=0.2, the associated phase velocity and *TCF* are 6 334 m/s and −33.3 ppm/°C, respectively.

Fig.6 shows the phase velocity, K^2, and *TCF* curves of the Sezawa mode SAW in the (100) AlN/(100) ZnO/IDTs/diamond structure as a function of H/λ at different R_h. (100) ZnO/DTs/diamond and (100) AlN/IDTs/diamond structures are two extreme cases for the (100) AlN/(100) ZnO/IDTs/diamond structure when the R_h ratio equal to 0 and infinity, respectively. The phase velocity and *TCF* curves of (100) AlN/IDTs/(100) ZnO/diamond structure (in Fig.6(a) and (c)) are similar to those of the other two structures. The K^2 value is lower than those in the other structures and serious dispersion occurs when large K^2 values are obtained, as shown in Fig.6(b). Large dispersion requires an exact control of the piezoelectric film thickness in order to ensure a high K^2 value, which causes difficult for the fabrication of the SAW devices.

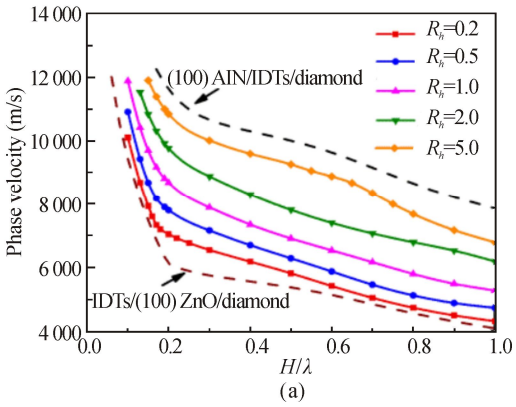

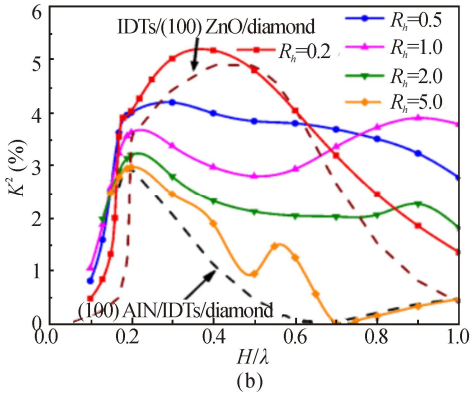

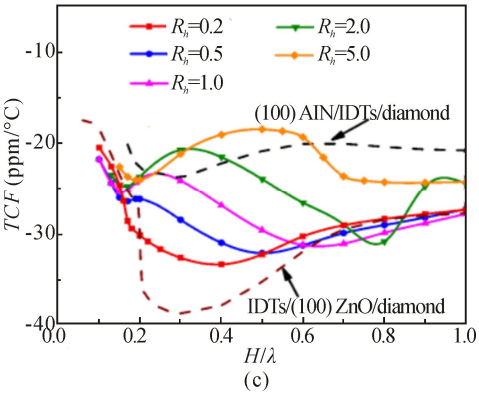

Fig.5 Calculated (a) phase velocity, (b) K^2, and (c) *TCF* for the Sezawa mode of SAW as a function of the H/λ in the (100) AlN/IDTs/(100) ZnO/diamond structure with different ratios of h_{AlN} to h_{ZnO}

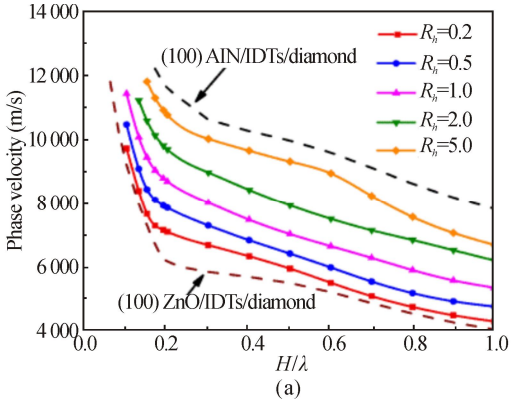

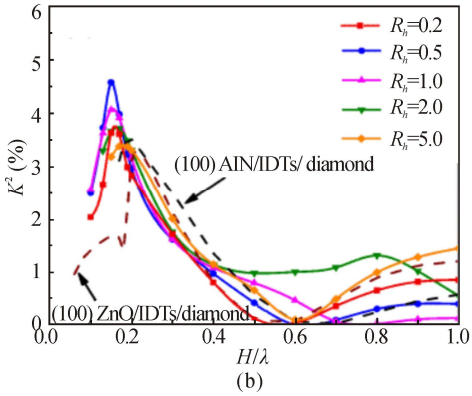

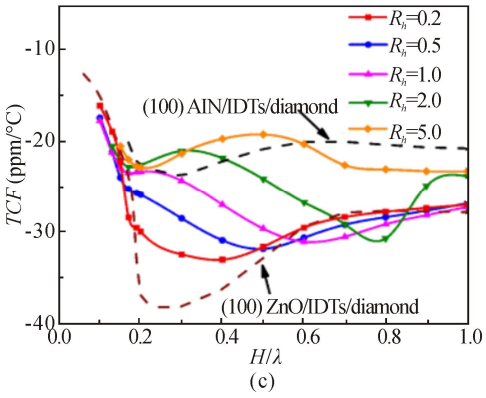

Fig.6 Calculated (a) phase velocity, (b) K^2, and (c) *TCF* for the Sezawa mode of SAW as a function of the *H*/*λ* in the (100) AlN/(100) ZnO/IDTs/diamond structure with different ratios of h_{AlN} to h_{ZnO}

The Rayleigh SAW propagation properties in (100) AlN/(100) ZnO/diamond layered structures are simulated by FEM. Three types of layered structures with different IDTs arrangements, which are IDTs/(100) AlN/(100) ZnO/diamond, (100) AlN/IDTs/(100) ZnO/diamond, and (100) AlN/(100) ZnO/IDTs/diamond structures, are considered. The phase velocity, K^2, and *TCF* of the first three SAW modes (M0, M1, and M2) are calculated and discussed. The results show that the Sezawa mode (M1) exhibits the largest K^2 of the first three SAW modes. The position of IDTs has slight influence on the phase velocity and *TCF* but great influence on the K^2. The (100) AlN/IDTs/(100) ZnO/diamond structure exhibits better SAW properties including high phase velocity and K^2 in the three structures. Furthermore, for the (100) AlN/IDTs/(100) ZnO/diamond structure, the exposed surface is AlN film, which possesses well chemical and thermal stability and can provide protection for the IDTs in the practical application. The simulated results show the high SAW performances of (100) AlN/(100) ZnO/diamond layered structure, and this structure possesses great potential in 5G wireless system.

Ethics declarations

Conflicts of interest

The authors declare no conflict of interest.

References

[1] SU R, SHEN J, LU Z, et al. Wideband and low-loss surface acoustic wave filter based on 15° YX-LiNbO/SiO/Si structure[J]. IEEE electron device letters, 2021, 42(3): 438-441.

[2] SHEN J, FU S, SU R, et al. High-performance surface acoustic wave devices using LiNbO/SiO/SiC multilayered substrates[J]. IEEE transactions on microwave theory and techniques, 2021, 69(8): 3693-3705.

[3] KADOTA M, ISHII Y, TANAKA S. Surface acoustic wave resonators with hetero acoustic layer (HAL) structure using lithium tantalate and quartz[J]. IEEE transactions on ultrasonics ferroelectrics and frequency control, 2020, 68(5): 1955-1964.

[4] WU J B, ZHANG S B, CHEN Y, et al. Advanced surface acoustic wave resonators on $LiTaO_3/SiO_2$/sapphire substrate[J]. IEEE electron device letters, 2022, 43(10): 1748-1751.

[5] ZHANG H, WANG H. Investigation of surface acoustic wave propagation characteristics in new multilayer structure: SiO_2/IDT/$LiNbO_3$/diamond/Si[J]. Micromachines, 2021, 12(11): 1211-1286.

[6] KOBAYASHI Y, TSUCHIYA T, OKAZAKI M, et al. High-frequency surface acoustic wave resonator with ScAlN/hetero-epitaxial diamond[J]. Diamond and related materials, 2021, 111(1): 108190.

[7] XIE B W, DING F Z, DONG Z B, et al. FEM analysis of piezoelectric film as IDT on the diamond substrate to enhance the quality factor of SAW devices[J]. Diamond and related materials, 2020, 102: 107659.

[8] LI M. High performance SAW resonators using $LiTaO_3/SiO_2$/4H-SiC multilayer substrate[J]. IEEE electron device letters, 2022, 43(10): 1772-1775.

[9] SUZUKI M, KAKIO S. Analysis of leaky surface acoustic wave characteristics propagating on high piezoelectric ScAlN film/high velocity quartz substrate[J]. Japanese journal of applied physics, 2020, 59(SK): SKKC07.

[10] MOUSTAFA M, LAOUINI G, ALZOUBI T. Finite element analysis of SAW sensor with ZnO substrate for dichloromethane (DCM) gas detection[J]. Archives of acoustics: journal of Polish academy of sciences, 2021, 46(3): 419-426.

[11] RO R, LEE R, LIN Z X, et al. Surface acoustic wave characteristics of a (100) ZnO/(100) AlN/diamond structure[J]. Thin solid films, 2013, 529: 470-474.

[12] QIAN L, LI C, LI M, et al. Theoretical investigation of surface acoustic wave propagation characteristics in periodic (AlN/ZnO)N/diamond multilayer structures[J]. Applied physics letters, 2014, 105(18): 183501.

[13] KVASHNIN G M, SOROKIN B P. Peculiarities of energy trapping of the UHF elastic waves in diamond-based piezoelectric layered structure. II. Lateral energy flow[J]. Ultrasonics, 2021, 111: 106311-106313.

[14] QIAN J, LI C P, QIAN L R, et al. Three-dimensional finite element simulation of love mode surface acoustic wave in layered structures including ZnO piezoelectric film and diamond substrate[J]. Diamond and related materials, 2018, 88: 123-128.

[15] WU S, LIN Z X, RO R, et al. Rayleigh and shear horizontal surface acoustic properties of (100) ZnO films on silicon[J]. IEEE transactions on ultrasonics ferroelectrics & frequency control, 2010, 57(5): 1237-1239.

[16] LIN Z X, WU S, RO R, et al. Surface acoustic wave properties of (100) AlN films on diamond with different IDT positions[J]. IEEE transactions on ultrasonics ferroelectrics & frequency control, 2009, 56(6): 1246-1251.

[17] HAKIKI M E, ELMAZRIA O, ASSOUAR M B, et al. ZnO/AlN/diamond layered structure for SAW devices combining high velocity and high electromechanical coupling coefficient[J]. Diamond & related materials, 2005, 14(3-7)：1175-1178.

[18] BRIZOUAL L L, ELMAZRIA O, ZHGOON S, et al. AlN/ZnO/diamond waveguiding layer acoustic wave structure：theoretical and experimental results[J]. IEEE transactions on ultrasonics ferroelectrics & frequency control, 2010, 57(8)：1818-1824.

[19] HAN X, WANG F, ZHANG K, et al. Effect on coupling coefficient of diamond-based surface acoustic wave devices using two layers of piezoelectric materials of different widths[J]. Diamond and related materials, 2022, 125：125-128.

[20] CHEN Y P, ZHAO J X, YANG Y J, et al. Substrate removal structures for AlScN/diamond surface acoustic wave resonators[J]. Diamond and related materials, 2023, 133.

[21] HATASHITA K, TSUCHIYA T, OKAZAKI M, et al. High electro-mechanical coupling coefficient SAW device with ScAlN on diamond[J]. Japanese journal of applied physics, 2023, 62.

[22] CUI Y, DU G, ZHANG Y, et al. Growth of ZnO (002) and ZnO (100) films on GaAs substrates by MOCVD[J]. Journal of crystal growth, 2005, 282(34)：389-393.

[23] WANG H H. Properties of AlN (100) thin films prepared by reactive laser ablation[J]. Modern physics letters B, 2008, 15(24)：1069-1075.

[24] DAS A, RATH M, NAIR D R, et al. Realization of preferential (100) oriented AlN thin films on Mo coated Si substrate using reactive RF magnetron sputtering[J]. Applied surface science, 2021, 3：149308.

[25] TIWARI C, DIXIT A. Highly textured (100)-oriented AlN thin films using thermal atomic layer deposition and their electrical properties[J]. Applied physics A, 2021, 127(11)：1-6.

[26] ZHANG Q, TAO H, TANG G, et al. SAW characteristics of AlN/SiO_2/3C-SiC layered structure with embedded electrodes[J]. Ultrasonics symposium IEEE, 2015, 63(34)：1608-1612.

[27] ZHOU C, YANG Y, CAI H, et al. Temperature-compensated high-frequency surface acoustic wave device[J]. IEEE electron device letters, 2013, 34(12)：1572-1574.

[28] LUO J T, QUAN A J, LIANG G X, et al. Love-mode surface acoustic wave devices based on multilayers of TeO_2/ZnO (1120)/Si (100) with high sensitivity and temperature stability[J]. Ultrasonics, 2017, 75(75)：63-70.